Biochemistry and Biophysics Reports 13 (2018) 32–38

Contents lists available at ScienceDirect

Biochemistry and Biophysics Reports

journal homepage: www.elsevier.com/locate/bbrep

Zo-peroxidase: Crystal structure and sequence of a highly-glycosylated peroxidase resistant to high concentrations of H_2O_2 from Japanese radish

Nizaá Jiménez-Arroyo, Paloma C. Gil-Rodríguez[1], Adelaida Díaz-Vilchis, Sonia P. Rojas-Trejo, Enrique Rudiño-Piñera*

Departamento de Medicina Molecular y Bioprocesos, Instituto de Biotecnología, Universidad Nacional Autónoma de México, Avenida Universidad 2001, Colonia Chamilpa, Cuernavaca, Morelos 62210, Mexico

ARTICLE INFO

Keywords:
Glycosylated protein structure
Hydrogen peroxide tolerance
Oxidase
Plant peroxidase
Redox enzyme

ABSTRACT

Understanding Peroxidase (PRXs) enzymatic diversity and functional significance from a three-dimensional point of view is a key point for structural and mechanistic studies. In this context, Zo-peroxidase (ZoPrx) a member of the class III peroxidases and secreted by plants, differs from all previously described PRXs because of its remarkable catalytic stability in the presence of hydrogen peroxide. In this work, we present the crystallographic structure of ZoPrx isolated from Japanese radish, at 2.05 Å resolution. The mature enzyme consists of a single monomer of 308 residues exhibiting the same fold as all previously described members of the plant PRXs superfamily. Furthermore, the enzyme contains a heme *b* group as the prosthetic group and two Ca^{2+} binding sites. Moreover, seven *N*-glycosylation sites were found in the structure, and 49 glycans bound to the two ZoPrx molecules found in the asymmetric unit are clearly visible in the electron density map. The comparison of ZoPrx coordinates with homologous enzymes revealed minor structural changes, in which the residue 177 appears to be responsible for enlarging the access to the heme cavity, the only structural finding which may be related to the H_2O_2 tolerance of ZoPrx and detected by X-ray crystallography. Because of its characteristics, ZoPrx has a broad range of potential applications from chemical synthesis to environmental biocatalysis, thus its aminoacidic sequence, partially completed using the electron density, and the three-dimensional structure itself, become a possible starting point to engineering heme-peroxidases to enhance oxidative stability.

1. Introduction

Peroxidases (PRXs, EC 1.11.1) are oxidoreductases present in bacteria, fungi, plants and animals. They use hydrogen peroxide (H_2O_2) to catalyze the oxidation of a wide variety of organic and inorganic substrates, from other proteins to small aromatic molecules, or from large polymers to inorganic ions. All PRXs studied to date share a similar catalytic cycle [1]; the general reaction goes as:

$$2RH + H_2O_2 \rightarrow 2R^{\bullet} + 2H_2O$$

PRXs have aroused interest from a biotechnological perspective for some time; these enzymes compel a large range of applications, from chemical synthesis to environmental biocatalysis. PRXs prosthetic group is one ferriprotoporphyrin IX commonly known as heme *b* [2]. According to their sequence identities and three-dimensional structures, heme peroxidases (hPRXs, EC 1.11.1.7) have been classified in two superfamilies. The first includes vertebrate enzymes and was named as the peroxidase-cyclooxygenase superfamily [3]. Meanwhile the second superfamily comprising bacteria, fungi and plant enzymes is known as the peroxidase-catalase superfamily. Additionally, to these superfamilies, three PRXs families are also described: di-heme peroxidases, dyp-type heme peroxidases and haloperoxidases [4].

The peroxidase-catalase superfamily is the most studied to date. Members of this superfamily, exhibit a conserved fold, contain as prosthetic group the heme *b* and are divided into three classes. The class I, integrated by prokaryotic intracellular enzymes (i.e. yeast cytochrome C peroxidase, CcP); class II that groups extracellular enzymes from fungi (i.e. lignin peroxidase, LiP); and the class III (POXs) which includes all secreted plant peroxidases (i.e. horseradish peroxidase isoenzyme C, HRPC) [1,2,5].

POXs are monomeric enzymes of ~ 300 amino acid residues [6], fundamentally involved in cell elongation, cell-wall formation and self-defense against various pathogen agents [7]. POXs also contain two hepta-coordinated calcium binding sites, four disulfide bridges, one salt

* Corresponding author.
E-mail address: rudino@ibt.unam.mx (E. Rudiño-Piñera).
[1] Current address: Case Western Reserve University, School of Medicine, Department of Physiology and Biophysics, Cleveland, OH, USA.

https://doi.org/10.1016/j.bbrep.2017.09.008
Received 13 June 2017; Received in revised form 24 August 2017; Accepted 24 September 2017
Available online 13 December 2017

bridge invariably localized on an aspartic acid and an arginine (Asp99 and Arg123 for HRPC) and a signal peptide for secretion [5]. All members of the superfamily have the same helical fold independent of the presence (class II and III) or absence (class I) of the disulfide bridges and structural calcium ions [8]. POXs are highly glycosylated; the *N*-glycans linked to these enzymes reach up to 30% of the total protein mass. As an example, HRPC and Banyan Peroxidase (BP) have 8 and 7 glycosylation sites, respectively, that display the Asn-X-Ser/Thr (X is not Pro) sequon, which occurs in loop regions toward the enzyme exterior [9].

Every POX studied so far is susceptible to inactivation by its co-substrate H_2O_2, even in the presence of reducing substrates, because of the low oxidative stability of these hPRXs against catalytic concentrations of H_2O_2, although their susceptibility level differs from enzyme to enzyme [1]. However, the Zo-Peroxidase (ZoPrx), a POX isoform isolated from roots of Daikon radish (Japanese radish *Raphanus sativus* L. var. *Longipinnatus*) has been described as naturally resistant to inactivation by H_2O_2 [10,11]. The mature enzyme consists of a single monomer of 308 residues exhibiting the same folding as the three members of the superfamily of plant PRXs. Additionally, it contains a heme *b* as the prosthetic group and two calcium binding sites within similar positions and deposited in the PDB (entries 6AS2, 1PA2, 1QO4 and 4CUO). In this work, we present the crystal structure of ZoPrx at 2.05 Å resolution and an analysis of its crystallographic structure. We emphasize on the putative role of the structure in regards the capacity of ZoPrx to resist inactivation by H_2O_2. In the structural determination, a complete sequence of ZoPrx was generated by fitting and refining the side chains into the electron density map following a mixed approach described below. The comparison of the ZoPrx three-dimensional structure with structurally homologous enzymes like *Arabidopsis* anionic peroxidase 2 (ATP A2, PDB entry 1PA2) and HRPC (PDB entry 1ATJ) point to the single variation of residue 177, located in the substrate access crevice near the prosthetic group, resulting in a potential bigger aperture toward the heme group reported in the available three-dimensional structures of POXs deposited in the PDB.

2. Materials and methods

2.1. Enzyme MS and crystallization

ZoPrx was isolated from fresh radishes as previously reported and its monomeric nature was tested by gel filtration analysis [11]. Mass spectrometry analysis and identification of the resultant sequences were carried out as described in Gil-Rodríguez et al. [10]. The SDS-PAGE bands of purified enzyme, used in this work, were digested with pepsin instead of trypsin.

Crystals were grown by hanging drop vapor-diffusion method after testing and generating several specific matrices based on *Crystal Screen I* and *II* kits from Hampton Research (Aliso Viejo, CA, USA) at 291 K. Drops were prepared manually in 24-well crystallization plates by mixing the enzyme (2 µl) at 50 mg ml^{-1} (in 10 mM sodium phosphate, pH 6.1) with the reservoir solution (2 µl) containing 0.1 M MES, pH 6.5% and 20% PEG 6000. Crystals suitable for data collection appeared after six weeks and were flash-cooled by immersion in liquid nitrogen exchanging water in the reservoir solution with 20% PEG 200 as cryoprotectant.

2.2. Data collection, data processing, and model refinement

A single diffraction data set was collected from a single crystal at 100 K on beamline X6A of the National Synchrotron Light Source (NSLS), using an ADSC Quantum 270 detector. The diffraction data set was indexed, integrated and scaled using the HKL-2000 suite [12]. Phases were determined by molecular replacement using the program MOLREP [13] with the coordinates from ATP A2 (PDB entry 1PA2) as a search model. The resulting model was improved by rigid-body refinement followed by restrained refinement with REFMAC [14]. The full sequence of ZoPrx was estimated by evaluating the fit of the model to the $2F_O - F_C$ electron-density map. Program COOT [15] was used for manual model building and addition of calcium ions, glycans and water molecules. Glycosylation sites were previously monitored using GlyProt [16]. All further refinement was performed with PHENIX [17] to a final R_{work}/R_{free} of 16.2/19.7%. Data collection and refinement statistics are summarized in Table 1.

Table 1
Summary of crystallographic data collection and refinement. Values in parentheses are for the highest resolution shell.

Parameters	ZoPrx PDB (6AS2)
Data collection statistics	
X-ray source	*BNL NSLS Beamline X6A*
Wavelength (Å)	*1.73*
Space group	$P12_11$
Unit-cell dimensions	
a, b, c (Å)	*59.1, 41.1, 137.8*
α, β, γ angles (°)	*90.0, 96.9, 90.0*
Resolution range (Å)	*30.0–2.05 (2.09–2.05)*
Unique reflections	*51,917*
Completeness (%)	*98.6 (99.2)*
Mosaicity	*0.3*
R_{sym} (%)[a]	*8 (50)*
Solvent content (%)	*53.0*
I/σ(I)	*21.6 (3.5)*
Multiplicity	*6.1 (6.4)*
Asymmetric unit content	*2 monomers*
Refinement statistics	
R_{work}/R_{free} (%)	*16.2/19.7*
B-value ($Å^2$)	
Protein	*30.7*
Water	*40.4*
Heme	*26.6*
Calcium ions	*25.7*
Glycans	*55.2*
PEG fragments	*55.3*
Wilson plot B-value ($Å^2$)	*30.8*
RMSD from ideal stereochemistry	
Bond lengths (Å)	*0.02*
Bond angles (°)	*1.75*
Coordinate error (Maximum-Likelihood Base) (Å)	*0.24*
Ramachandran plot (%)	
Most favored regions	*98.46*
Additional allowed regions	*1.37*
Disallowed regions	*0.17*

[a] $R_{sym} = \Sigma_{hkl} \Sigma_i |I_i(hkl) - (I(hkl))| \Sigma_{hkl} \Sigma_i I_i (hkl)$, where $I_i(hkl)$ and $(I(hkl))$ represent the diffraction-intensity values of the individual measurements and the corresponding mean values. The summation is over all unique measurements.

2.3. Sequence-structure comparison with homologous enzymes

Initially, a preliminary sequence for ZoPrx based on known sequence segments of ZoPrx filling the unknown residues with ATP A2 sequence was used to search similar regions within available sequences to find homologous enzymes through the EBI NCBI-BLAST [18]. The PDB and the EBI's UniProt (http://www.uniprot.org) were employed to find protein sequences with at least 50% sequence identity with the preliminary sequence of ZoPrx. From the search in the PDB, all the enzymes (all been hPRXs) which had an identity greater than 40% (eight enzymes collectively referred as 8POXs) were selected. From the search within the UniProt, only the first 50 sequences (all been hPRXs) sharing an identity up to 58% were used. A multiple sequence alignment (MSA) was carried out using *MView* [19] with ZoPrx's preliminary sequence as a seed, the 8POXs from the PDB and the 50 hPRXs from UniProt were used to complete the ZoPrx sequence over the electron density map fitting. To identify residue 177 a simulated annealing omit map were performed using the final phases; additionally, residues Arg, Gln, His, Lys, Val, Ser and Thr were modeled and their $2F_O - F_C$ and F_O

$-F_C$ maps were carefully analysed, as well as the neighboring atoms potentially capable to interact with the atoms of each potential residue at position 177. Once the final sequence was proposed, it was compared against the 8POXs sequences to highlight regions with lower or higher identity. To find structural similarities/differences among ZoPrx a structural alignment with its homologous was carried out in COOT and CCP4mg [20].

3. Results

3.1. Crystal structure and sequence

The crystal structure of native ZoPrx from Japanese radish *Raphanus sativus* L. Daikon was determined at 2.05 Å resolution with a final R_{work}/R_{free} of 16.2/19.7% (Table 1). Calculations for Matthews coefficient support the presence of two monomers within the asymmetric unit (V_m = 2.61 Å^3 Da^{-1}) [21,22].

The sequence for ZoPrx was partially obtained (111 out of 308 residues) from two sequencing mass spectrometry performed [10] and this work. The rest of the sequence was obtained through manual adjustment of the structural model over the electron density map in conjunction with a consensus in agreement with the sequence alignment of 8POXs and other 50 hPRXs with at least 58% of sequence identity. From all modeled residues, 24 of them were adjusted according to the consensus, given that the $2F_O - F_C$ map was not capable of discerning the identity of the side chain to be modeled. The final consensus sequence of ZoPrx with a total of 308 residues is presented in Supplementary material Fig. S1.

As predicted by Gil-Rodríguez et al. [10], ZoPrx is an acidic oxidoreductase from class III superfamily of peroxidase-catalases, according to its final consensus sequence, with a monomeric behavior confirmed by gel filtration analysis and by its crystallographic structure [11] and this work. Additionally, the overall architecture of ZoPrx is identical to those of typical plant peroxidases [23]. The three-dimensional structure of ZoPrx comprises 14 α-helices A to J (Supplementary material Fig. S1 and Fig. 1) as well as additional helices B′ (Pro71-Ala73), D′ (Gln133-Ser139), F′ (Cys178-Leu185) and F″ (Thr200-Leu209), however, not all graphical programs used here detected F′ as a helix. ZoPrx also has two short anti-parallel β-strands, the β1 (Arg175-Ala176) and the β2 (Thr220-Asn221).

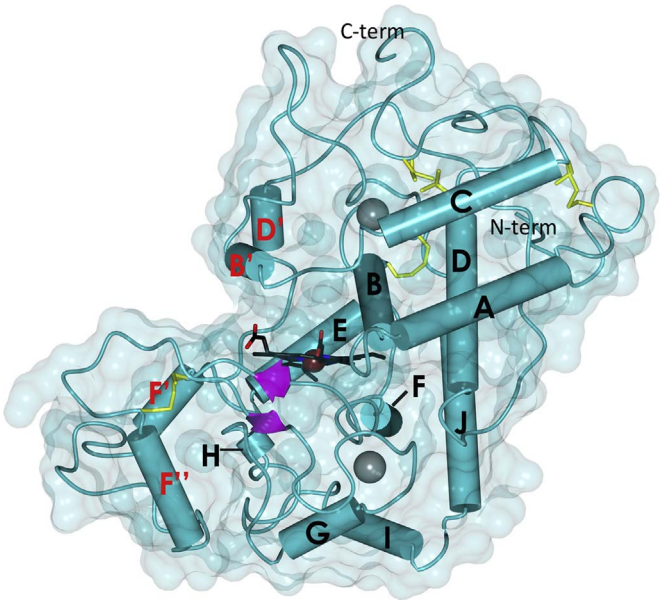

Fig. 1. Crystal structure of ZoPrx. Conserved α-helices A–J are shown labelled in black, plus additional α-helices B′, D′, F′ and F″ labelled in red. β-sheets appear in magenta. Disulfide bridges are indicated in yellow and bound calcium ions appear as gray spheres. This Richardson representation corresponds to molecule A from the asymmetric unit, oriented in a way that the heme group (in black, Fe ion as a cherry sphere) marks a horizontal division between domain I (top) and domain II (bottom) of the enzyme.

3.2. Active site, Ca^{2+} ions and disulfide bridges

ZoPrx structure in its native state has a heme *b*-containing active site with a Fe ion coordinated by His171 at 2.2 Å. The nearest water molecule in the distal cavity is at 3.9 Å from the Fe ion.

Two structural conserved calcium ions are present in both copies of ZoPrx in the asymmetric unit. The distal hepta-coordinated Ca^{2+} is positioned at 15.7 Å from the Fe ion. Its seven ligands are O and O_D from Asp45, O from Val148, O from Gly50, O_D from Asp52, O_G from Ser54 and a water molecule. The proximal Ca^{2+} is positioned at 13.4 Å from the Fe ion, and it is also hepta-coordinated with O from Thr172, O_G from Thr171, O_{D2} from Asp223, O from Thr226, O_G from Thr226, O from Ala229 and O_D from Asp231. The distance between both Ca^{2+} ions is 26.7 Å.

The eight cysteine residues within the ZoPrx sequence (Cys13, −46, −51, −93, −99, −178, −210 and −301) form four disulfide bridges which confer higher rigidity to the enzyme [2]. Also, a buried salt bridge formed by residues Asp101 and Arg125 is present. Those are typical features of class II and III plant peroxidases alongside the presence of the two calcium-binding sites [2,5].

3.3. Glycosylations

Electron density maps corresponding to *N*-linked glycosylations (*N*gly) were observed at seven different sites (Asn5, −15, −137, −149, −187, −199 and −269) from eight potential *N*gly sites (*N*gly for Asn306 was not found in the electron density map) predicted with GlyProt [16]. The seven *N*gly sites have the sequon Asn-X-Ser/Thr (X not Pro). Each *N*-glycan chain (composed of *N*-acetylglucosamine or GlcNAC, fucose, mannose and xylose) resulted different both in size and position, given the adjustment of the observed electron density map for each site. The longer form of all the determined glycan for ZoPrx possesses the structure Manα3(Xylβ2)-Manβ4GlcNAcβ4(Fucα3)GlcNAc-. This structure could correspond to complex-type *N*-glycans or truncated-type *N*-glycans [24,25]. From all POXs with available crystallographic structure, ZoPrx has, by far, the largest number of modeled *N*-glycans deposited in the PDB (49 in total). In comparison, some of the 8POXs showed *N*gly sites, none of them is as complete as it is seen in ZoPrx crystallographic structure. Nine *N*gly sites have been predicted for ATP A2 [26] from which seven correspond to those found for ZoPrx. HRPC has eight *N*-glycans [27] from which only three correspond in location to ZoPrx; BP [9] and SBP have seven *N*-glycans [28] each, but only two correspond in location to two *N*-glycans of ZoPrx for both enzymes. RPTP and PNP have nine and three *N*gly sites, respectively [29,30] but only one is shared by ZoPrx in both cases. These observations remark the high variability, regarding *N*gly, among 8POXs.

Each one of the seven *N*gly sites found in ZoPrx is positioned in solvent-exposed loop regions (Fig. 2). All these *N*gly sites aim toward the outside of the molecule and are distributed uniformly across the enzyme surface, suggesting that its major purpose seems to improve the solubility of the enzyme and potentially increasing the protein cross-linking mediated by free radicals [31,32]. The location of the glycosylations on the structure suggests that glycans have no effect on the activity of ZoPrx, but may affect its stability, as pointed by Tams and Welinder [33], who reported that the deglycosylation of HRPC did not affect its activity but modified its solubility and stability against proteolysis. The Asn149-glycan binding site is at about 11 Å from the heme exposed δ-meso edge. However, the active site's distal cavity is protected by the side chains of Gln145 and Ile150 residues in this glycosylated site. In agreement with Schuller et al. [31], this oligosaccharide might interfere with the union of large molecules to the distal cavity of the enzyme (as postulated for PNP), although it may not influence the

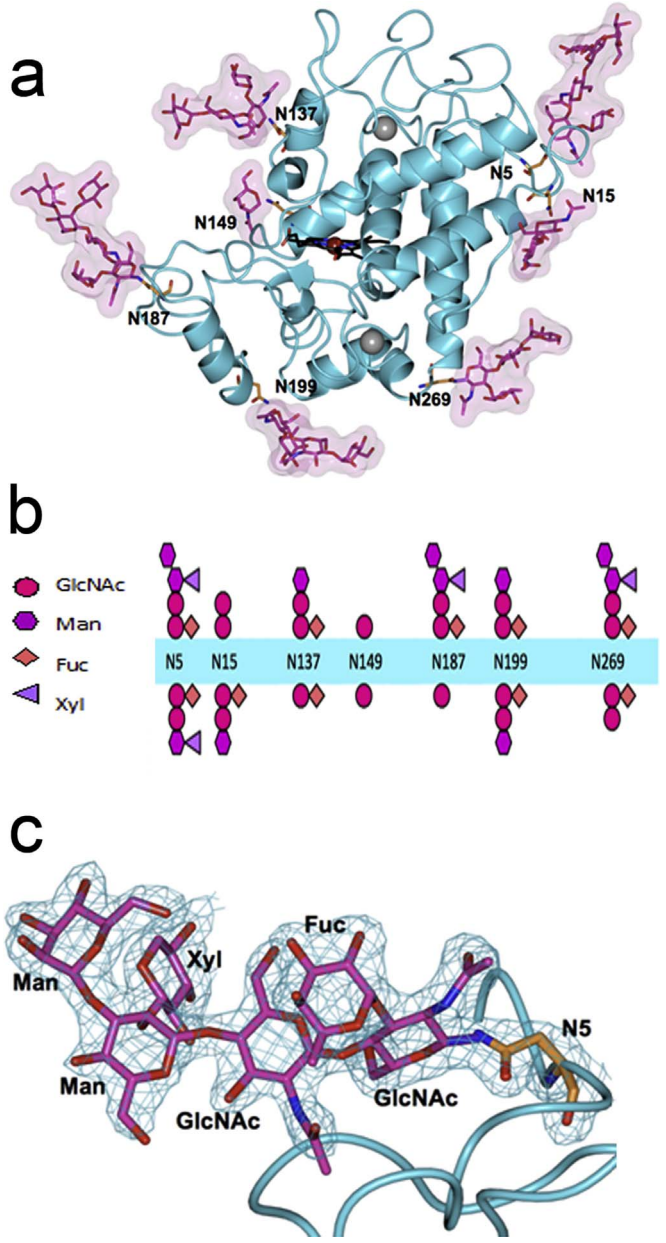

Fig. 2. *N*-glycan chains found in native ZoPrx. (a) Ribbon representation of ZoPrx showing the seven *N*-linked glycan chains (pink) covalently attached to their respective asparagine residue (orange). Both sugars and asparagines are shown in stick representation. (b) Schematic drawing of the glycosylation pattern of ZoPrx. Sugar chains attached to *N*-glycosylation sites of molecule A, from the asymmetric unit, of the heme-peroxidase point up whereas those of molecule B, the second monomer found into the asymmetric unit, point down. (c) Detailed view of the ZoPrx $2F_O - F_C$ electron density map around Asn5 and countered at 1 σ.

access of smaller substrates to the heme edge.

3.4. Sequence-structure comparison with homologous enzymes

The structural alignment showed that ZoPrx has the same typical fold of class III plant PRXs as all 8POXs. In this work, the ATP A2 (PDB 1PA2) [34], BP (PDB 4CUO) [9], SBP (PDB 1FHF) [35], HRPC (PDB 1ATJ) [32], ATP N (PDB 1QGJ) [36], PNP (PDB 1SCH) [31], BP 1 (PDB 1BGP) [37] and RPTP (PDB 3HDL) [29] are collectively referred as 8POXs.

The three-dimensional structure of ZoPrx is almost identical to ATP A2, with an overall r.m.s.d. of 0.47 Å using 306 Cα atoms, sharing a sequence identity of 87% (Supplementary material Fig. S1). It is important to remark that the r.m.s.d. between both monomers of ZoPrx in the asymmetric unit is 0.38 Å using 306 Cα atoms, additionally the electron density in monomer A is better than in monomer B. Therefore, monomer A was selected to be used in our analysis. The r.m.s.d. and the sequence identity of the 8POXs regarding ZoPrx can be reviewed in Supplementary material Table S1. All the variant residues between ZoPrx and ATP A2 (39 residues) are accessible to the solvent exposed surface, except for Thr100 and Ser177 (Cys98 and Arg175 for ATP A2, respectively). This implies that the overall interior packing of both POXs is alike. ZoPrx and ATP A2 present a similar distribution of secondary structural elements: both POXs conserve helix B′ which has been proposed as common to class I and II peroxidases [32], but also helix F' which has not been described as an structural feature in POXs. All other helices (A-J) present lengths and positions almost identical to other homologous structures, although helix H is shorter in ZoPrx (Gln246-Asp248) respect to ATP A2 (Gln244-Ser251). Both β-strands in ZoPrx (Arg175-Ala176 and Thr220-Asn221) are only one residue shorter than in ATP A2 (Arg173-Arg175 and Ile217-Asn219).

The active site of ZoPrx, including the position of the heme group and relevant residues of the catalytic site (His44 and Arg40), are identical to the active site of ATP A2 and the rest of 8POXs. All 8POXs presenting the proximal His, and both distal His and Arg with overlapped positions. Since the work of Schuller et al. [31], it is believed that substrates interact with hPRXs through the heme exposed edge. Chemical modification with suicide substrate inhibitors shows that these substrate-like molecules covalently attach to the δ-meso heme carbon, which is oriented towards the access pathway that leads to the heme pocket [31]. Residues surrounding this substrate access channel in ZoPrx are Gly70, Pro71, Ala73, Ile140, Pro141, Ser142, Pro143, Thr144, Gln145, Ser177, Gly179, Val180, Ser182 and Leu245. The substrate access channel in ZoPrx exhibit several substitutions regarding ATP A2, such as ATP A2 → ZoPrx: Val71 → Ala73, Ile142 → Thr144, Glu143 → Gln145, Arg175 → Ser177 and Asn180 → Ser182, while all other residues in the access channel are conserved.

One common feature for all POXs is the presence of a hydrophobic pocket formed by a cluster of aromatic residues that enclose the heme group and cause a moderated projection of the segment corresponding to α-helices F′/F″ towards the solvent [29]. For ZoPrx, residues in the hydrophobic cavity are Phe43, Phe47, Gln145 and Phe154 on the distal side and Phe173, Leu222, Phe230 and Phe277 for the proximal side. The exchange of Phe for Gln (position 145 in ZoPrx) on the distal side; and for Leu (position 222 for ZoPrx) on the proximal side is also shared by ATP A2 and ATP N. Because of its hydrophilic nature, the Gln causes a compacting of the hydrophobic cavity and retraction of the helices F′/F″ projected segment [35].

The most notorious difference between the three-dimensional structures of ZoPrx and ATP A2 was found in a surface-exposed loop located between helices F″ and G. It has been described, that certain POXs contain a large insertion between helices F and G stabilized by a disulfide bridge, been, this insertion a hypervariable region [32]. By superposing the coordinates of ZoPrx and ATP A2 a variation can be seen (Fig. 3), which take place at the end of helix F″, just after Cys210 or Cys208, respectively. This variation occupies the position of the hypervariable region mentioned above. This loop between helices F″ and G are eight residues long for both, ZoPrx (Pro211-Thr219) and ATP A2 (Pro208-Thr216), although they differ by three residues. Moreover, by superposing the nine available three-dimensional structures of POXs (ZoPrx and 8POXs), a high variation of the structure of this loop for each enzyme is visible.

The heme *b* of POXs, interacts through hydrophobic contacts with all surrounding residues, both in the distal and proximal cavities. By comparing said residues for ZoPrx and ATP A2, only one different residue was found: residue 177 in ZoPrx. To unveil the identity of residue 177 in ZoPrx a simulated annealing omit map using the final phases and different refinements using Arg, Gln, His, Lys, Val, Ser and Thr in position 177 were performed. These residues were chosen according to the

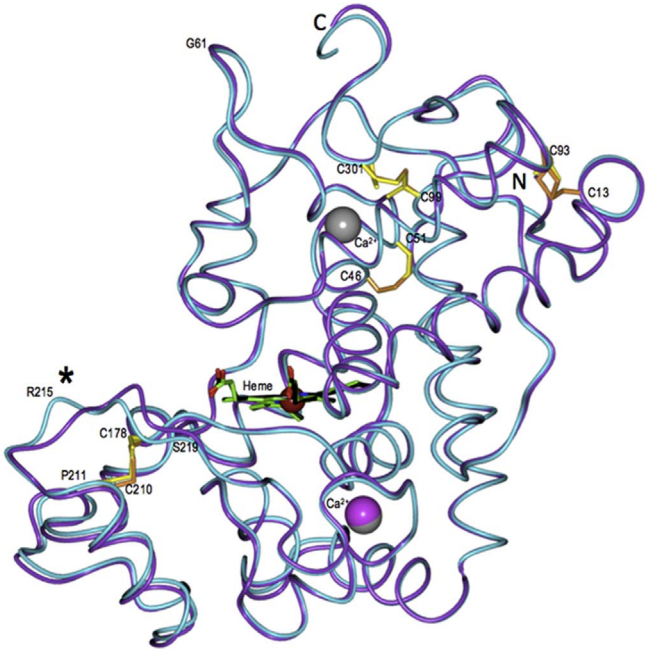

Fig. 3. Superimposed Cα trace of ZoPrx in light blue, and ATP A2 in purple. The loop that varies between the two enzymes localized between α-helices F″ and G is indicated with an asterisk. Disulfide bridges are in orange for ATP A2 and yellow ZoPrx. Bound calcium ions appear as spheres, in gray for ZoPrx and magenta for ATP A2. The heme group is showed in black for ZoPrx and in green for ATP A2. Numbered residues correspond to ZoPrx. The terminal ends are marked with N (N-term) and C (C-term).

sequence of 8POX, the 50 hPRXs sequences obtained from UniProt, the different electron densities attempted and the inspection of neighboring atoms. After these analyses, it is more likely that residue 177 is a Ser, or a Thr with a conformer not previously described at the PDB. A Lys may be fitted in the electron density map of ZoPrx monomer B, but not in monomer A of the asymmetric unit, been possible that a Lys occupies this residue, in monomer A and B, but with B values higher that 70 and 60 $Å^2$, respectively, in their N_Z, C_E and C_D atoms. Even if a Lys occupies position 177, their high B values may imply an unusual open access to the heme cavity. Arg, Gln, Val and His are not allowed according to the $F_O - F_C$ electron density maps. Thus ZoPrx residue 177 is more likely to be Ser; however, Thr or even Lys are not completely discarded (Supplementary material Fig. S2). This Ser177 is linked through a H-bond (by its N) to the propionate group linked to the heme C_{2A} by the O_{2A}. This residue differs from Arg175, the equivalent residue in ATP A2, where the propionate O_{2A} is forming two H-bonds, one with the N and one with the N_{H1} of said Arg. Ser177 from ZoPrx is part of the substrate access channel towards the active site. The analysis of Ser177 within the crystallographic structure shows the position of the lateral chain in front of the heme by looking through the aperture disposed by the structure towards the active site just at the access channel end. Seeing from the same perspective in ATP A2, it was found that the lateral chain of Arg175 forms a partial blockade on the aperture towards the heme group. Consecutively it was found that all 8POXs present one distinct residue equivalent to the position of Ser177 in ZoPrx. No other residue binds with the δ-meso edge propionate, although all form two H-bonds with the propionate. These bonds make the heme propionate-protein interaction, by one H-bond from Ser177 with propionate, unique for ZoPrx. The difference in the interaction between the δ-meso heme edge propionate and the polypeptide chain might influence the catalytic properties and stability of the enzyme [29]. The residues that differ from Ser177 for ZoPrx to the 8POXs are: for SBP, Arg175; HRPC, Gln176; ATP N, Lys171; PNP, Gln175; BP 1, His185; and 3HDL, His175. These residues vary in their side chain's properties, being hydrophilic (Ser or Gln) or basic (Arg, Lys or His).

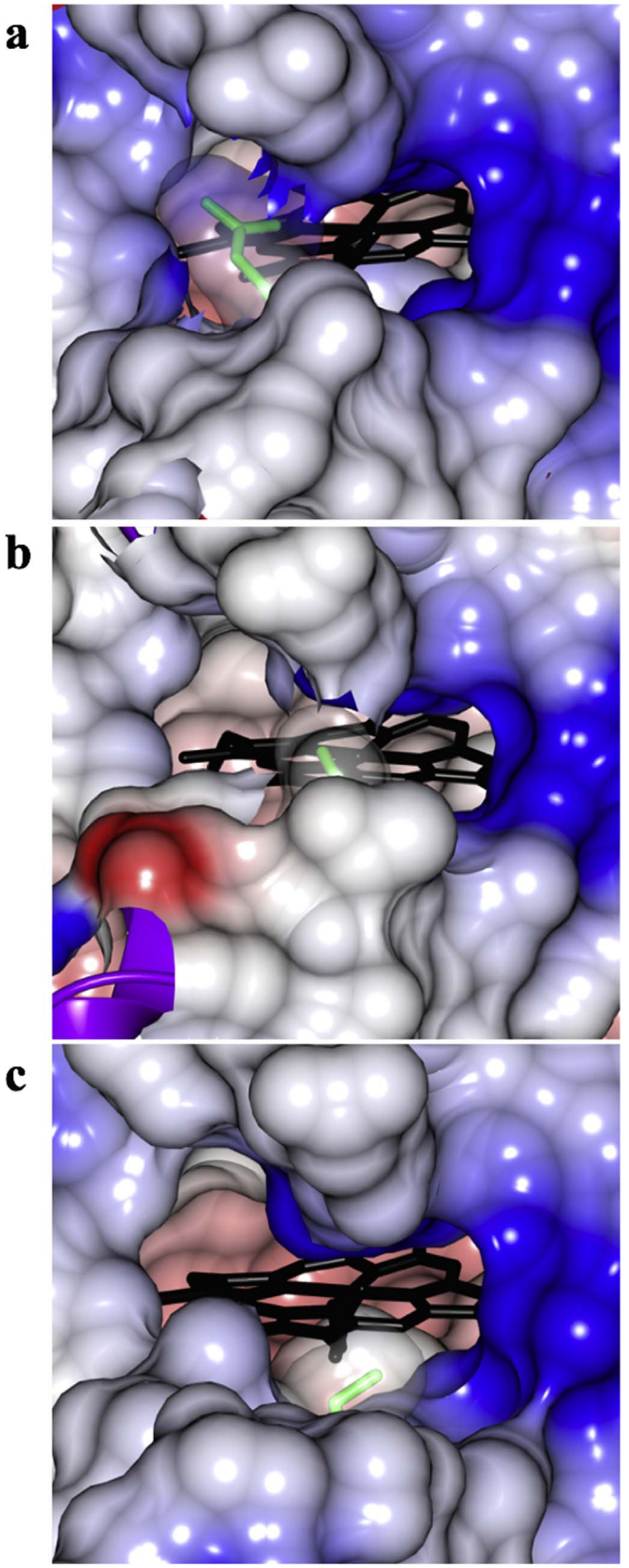

Fig. 4. Electrostatic surface calculations in the vicinity of the heme within (a) ATP A2, (b) PNP and (c) ZoPrx, oriented toward the substrate access channel. In each image, the residue at the end of the access channel localized in front of the δ-meso heme edge that forms a partial vertical blockade (Arg175 for ATP A2 and Gln176 for PNP) or not (Ser177 conformer B for ZoPrx) is colored in green. The electrostatic surface is colored as red when the charge of the residue is ≥ 1 eV, or blue when the charge is ≤ −1 eV, otherwise, it remains white.

Although the common feature is the relatively long side chains which are partially blocking the access to the δ-meso heme edge. This has been seen in a representation of the electrostatic surface of each crystallographic structure, in contrast with the side chain of Ser177 in ZoPrx (Fig. 4). Due to the presence of Ser177, the overall area of access to the channel end for ZoPrx is ~ 12 $Å^2$ while the equivalent area for ATP A2 is ~ 4 $Å^2$ (estimated with MOLEOnline version 1.4 [38]). The three-fold increase in the aperture of the channel might be involved in the resistance of ZoPrx to high concentrations of H_2O_2; however, the identification of ZoPrx residue 177 as a Ser needs to be confirmed.

4. Discussion

Heme-peroxidases have attracted the attention of many researchers, especially due to their broad distribution among species, and for their great variety of physiological roles. To date, the biggest limitation for their exploitation has been to achieve higher recombinant expression and to yield better stability for these enzymes. Every year, the availability of new three-dimensional structures, especially POXs, increases the possibility of understanding why there is a high occurrence of multiple isoenzymes of PRXs and their physiological relevance [39]. The main challenge is using the new structural information to explain the important physiochemical disparities among members of the class III PRXs.

ZoPrx was isolated from roots of Japanese radish. Since ZoPrx represent only 1.5% of the peroxidase activity within the crude extract, to purify a significant quantity (> 1 mg of protein), a batch of Japanese radishes (50 kg yield ~ 1 mg) is required [11], thus presenting great limitation for crystallization trials. Obtaining the complete sequence of ZoPrx facilitates the possibility to obtain a major quantity of enzyme through recombinant DNA technologies, which theoretically would yield an easier-to-crystallize active enzyme without glycosylations. However, it is likely that the proposed sequence may not be correct in its totality. To model a three-dimensional crystallographic structure; it is crucial to count with the complete protein sequence to adjust and refine each residue in agreement to the respective electron density map. For ZoPrx, we only had a partial sequence. Therefore, the majority of the modeling was made according to the obtained electron density; from the 308 residues of ZoPrx, 284 were assigned with an unappealable structural foundation. Because the map resolution (2.05 Å) presented some uncertainty for the identity of several residues within the model, it was necessary to conduct a consensus with homologous sequences to complete the sequence of ZoPrx, thus its final sequence may not be 100% reliable.

According to their three-dimensional coordinates, ZoPrx invariably present, as all plant PRXs investigated so far, two distinct structural domains. These domains envelope the heme *b* group located within a cavity formed by two antiparallel α-helices B and F. Helix F in domain II provides the conserved proximal His171, whose N_D is linked by an H-bond to the carboxylate group of a conserved Arg248. Meanwhile, helix B in domain I forms the active site's distal cavity and provides the invariable His and Arg (His44 and Arg40) that are crucial for the heterolytic cleavage of the peroxidic bond in H_2O_2.

Despite the few changes in residues in the substrate access channel between ZoPrx and the 8POXs, the hydrophobic nature of the substrate access channel is maintained, which is another feature of POXs. For ZoPrx, the most relevant residue change on said channel is a Ser177, located in the extreme of the channel in front of the heme moiety. Ser177 only forms one H-bond with the δ-meso edge propionate of the prosthetic group, which differs from the 8POXs in which their equivalent residues form two H-bonds with the same propionate. The catalytic activity of hPRXs is influenced by the proper orientation of the heme group regarding the protein adjacent residues. That is why the heme propionate groups have an important role in the stability of the active site cavity and the formation of catalytic intermediaries [29]. Moreover, several studies suggest that the propionate groups act as an electrostatic anchorage point for the correct binding and orientation of the heme with the polypeptide chain as well also influencing its electronic properties [40]. Guallar and Olsen [41] suggested that the propionates participate in the electronic transference of the H_2O_2 to the iron ion. The electron transference mechanism is a delicate balance between non-coupled pairs in the propionate orbitals and the porphyrin π system. Thus, it is expected that the enzyme topology would affect (deactivating or activating) said balance. That is why the change in the interaction propionate-protein mediated by Ser177 could be influencing the catalytic properties of the POX to some degree and consequently, this might be related to the exhibited resistance of ZoPrx towards inactivation by H_2O_2. Furthermore, unlike all 8POXs that present residues with a larger side chain in the same location, the Ser177 (for ZoPrx) does not form a partial vertical blockade on the heme access. Before confirming or denying this features as the responsible (at least partially) for the intrinsic resistance towards inactivation by H_2O_2 in ZoPrx, it would be necessary to implement cloning with site-directed mutagenesis. The mutation of the Ser177, perhaps to Arg (as in ATP A2), to perform both activity assays and especially oxidative stability towards H_2O_2 assays, seems necessary to confirm our hypothesis.

It has been noted that protein glycosylation confers greater solubility and resistance against proteolysis. It has also been tested for PRXs that both the Ca^{2+} ions and *N*-glycans influence the stability of these enzymes. Although the role of the oligosaccharides in the control of the folding pattern is still unclear in contrast to the well explored structural role of the Ca^{2+} ions. The exploration of this matter has been hampered in great measure due to scarce crystallographic structures of glycoproteins showing glycans on the electron density maps, owing to inherent difficulties of crystallizing natively glycosylated proteins; the flexibility and heterogeneity of polysaccharide chains hinder the crystal's growth. There are cases like the one presented in this work, where it was possible to crystallize highly glycosylated native ZoPrx, in which case, we believe that the crystallization conditions were fortuitously conducive.

Acknowledgements

NJA was supported by an Undergraduate fellowship from UNAM and with a M.Sc. fellowship from CONACyT. ERP acknowledge financial support from Instituto de Biotecnología-UNAM. We are grateful to the staff at the BNL NSLS beamline X6A for data-collection facilities. The X6A beamline is funded by NIGMS (GM-0080) and the US Department of Energy (No. DE-AC02-98CH10886). The National Synchrotron Light Source, Brookhaven National Laboratory is supported by the US Department of Energy under contract No. DE-AC02-98CH10886.

Appendix A. Transparency document

Transparency document associated with this article can be found in the online version at http://dx.doi.org/10.1016/j.bbrep.2017.09.008.

Appendix B. Supplementary material

Supplementary data associated with this article can be found in the online version at http://dx.doi.org/10.1016/j.bbrep.2017.09.008.

References

[1] A. Hiner, J. Hernández, J.N. Rodríguez, M.B. Arnao, F. García, M. Acosta, Plant peroxidases from 3 classes share similar mechanisms of inactivation with peroxide, Plant peroxidases: biochemistry and physiology, in: Proceedings of the VI International Plant Peroxidase Symposium, Universidad de Murcia, Murcia, Spain, 2002, pp. 92–96.
[2] L. Banci, Structural properties of peroxidases, J. Biotechnol. 53 (1997) 253–263.
[3] M. Zamocky, C. Jakopitsch, P.G. Furtmüller, C. Dunand, C. Obinger, The peroxidase-cyclooxygenase superfamily: reconstructed evolution of critical enzymes of

the innate immune system, Proteins 72 (2008) 589–605.
[4] M. Zamocky, C. Obinger, Chapter 2, Molecular Phylogeny of Heme Peroxidases, Biocatalysis Based on Heme Peroxidases: Peroxidases as Potential Industrial Biocatalysts, Springer, USA, 2010.
[5] K.G. Welinder, Superfamily of plant, fungal and bacterial peroxidases, Curr. Biol. 388 (1992) 388–393.
[6] H.B. Dunford, Heme Peroxidases, Wiley, USA, 1999.
[7] S. Hiraga, K. Sasaki, H. Ito, Y. Ohashi, H. Matsui, A. Large, Family of class III plant peroxidases, Plant Cell Physiol. 42 (2001) 462–468.
[8] F. Ruiz-Dueñas, A.T. Martínez, Chapter 3, Structural and Functional Features of Peroxidases with Potential as Industrial Biocatalysts, Biocatalysis Based on Heme Peroxidases: Peroxidases as Potential Industrial Biocatalysts, Springer, USA, 2010.
[9] F. Passardi, C. Cosio, C. Penel, C. Dunand, Peroxidases have more functions than a Swiss army knife, Plant Cell Rep. 24 (2005) 255–265.
[10] P. Gil-Rodríguez, C. Ferreira-Batista, R. Vázquez-Duhalt, B. Valderrama, A novel heme peroxidase from *Raphanus sativus* intrinsically resistant to hydrogen peroxide, Eng. Life Sci. 8 (2008) 286–296.
[11] P. Gil-Rodríguez, B. Valderrama, An optimized procedure for the purification of Zo peroxidase (ZoPrx), a low abundance peroxidase from Japanese radish roots, Int. J. Plant Physiol. Biochem. 1 (2009) 9–12.
[12] Z. Otwinowski, W. Minor, Processing of X-ray diffraction data collected in oscillation mode, Methods in enzymology, 276: Macromolecular Crystallography, Part A, Academic Press, N.Y., USA, 1997.
[13] A.A. Vagin, A. Teplyakov, MOLREP: an automated program for molecular replacement, J. Appl. Crystallogr. 30 (1997) 1022–1025.
[14] G.N. Murshudov, A.A. Vagin, E.J. Dodson, Refinement of macromolecular structures by the maximum-likelihood method, Acta Crystallogr. D 53 (1997) 240–255.
[15] P. Emsley, B. Lohkamp, W.G. Scott, K. Cowtan, Features and development of Coot, Acta Crystallogr. D 66 (2010) 486–501.
[16] A. Bohne-Lang, C.W. von der Lieth, GlyProt: in silico glycosylation of proteins, Nucl. Acids Res. 33 (2005) 214–219.
[17] P.D. Adams, R.W. Grosse-Kunstleve, L.-W. Hung, T.R. Ioerger, A.J. McCoy, N.W. Moriarty, R.J. Read, J.C. Sacchettini, N.K. Sauter, T.C. Terwilliger, PHENIX: building new software for automated crystallographic structure determination, Acta Crystallogr. D 58 (2002) 1948–1954.
[18] T. Madden, Chapter 16, The BLAST Sequence Analysis Tool, The NCBI Handbook [Internet], 2nd ed., National Center for Biotechnology Information, Bethesda (MD), 2002.
[19] N.P. Brown, C. Leroy, C. Sander, MView: a web compatible database search or multiple alignment viewer, Bioinformatics 14 (1998) 380–381.
[20] S. McNicholas, E. Potterton, K.S. Wilson, M.E.M. Noble, Presenting your structures: the CCP4mg molecular-graphics software, Acta Crystallogr. D 67 (2011) 386–394.
[21] B.W. Matthews, Solvent content of protein crystals, J. Mol. Biol. 33 (1968) 491–497.
[22] K.A. Kantardjieff, B. Rupp, Matthews coefficient probabilities: improved estimates for unit cell contents of proteins, DNA, and protein-nucleic acid crystals, Protein Sci. 12 (2003) 1865–1871.
[23] L. Holm, C. Sander, The FSSP database: fold classification based on structure–-structure alignment of proteins, Nucl. Acids Res. (1996) 206–209.
[24] C. Rayon, P. Lerouge, The protein N-glycosylation in plants, J. Exp. Bot. 49 (1998) 1463–1472.
[25] I.B.H. Wilson, Glycosylation of proteins in plants and invertebrates, Curr. Opin. Struct. Biol. 12 (2002) 569–577.
[26] L. Nielsen, C. Indiani, A. Henriksen, A. Feis, M. Becucci, M. Gajhede, G. Smulevich, et al., Differential activity and structure of highly similar peroxidases, spectroscopic, crystallographic, and enzymatic analyses of lignifying *Arabidopsis thaliana* peroxidase A2 and horseradish peroxidase A2, Biochemistry 40 (2001) 11013–11021.
[27] K.G. Welinder, Amino acid sequence studies of horseradish peroxidase, Eur. J. Biochem. 502 (1979) 483–502.
[28] K.G. Welinder, Y.B. Larsen, Covalent structure of soybean seed coat peroxidase, Biochim. Biophys. Acta 1698 (2004) 121–126.
[29] L. Watanabe, P. Ribeiro, D. Moura, L. Bleicher, A.S. Nascimento, L.S. Zamorano, J.J. Calvete, et al., Crystal structure and statistical coupling analysis of highly glycosylated peroxidase from royal palm tree *Roystonea regia*, J. Struct. Biol. 169 (2010) 226–242.
[30] R.B. van Huystee, Y. Sun, B. Lige, A retrospective look at the cationic peanut peroxidase structure, Crit. Rev. Biotechnol. 22 (2002) 335–354.
[31] D.J. Schuller, N. Ban, R.B.V. Huystee, A. Mcpherson, T.L. Poulos, The crystal structure of peanut peroxidase, Structure 4 (1996) 311–321.
[32] M. Gajhede, D.J. Schuller, A. Henriksen, A.T. Smith, T.L. Poulos, Crystal structure of HRPC at 2.5 Å resolution, Nat. Struct. Biol. 4 (1997) 1032–1038.
[33] J.W. Tams, K.G. Welinder, Mild chemical deglycosylation of horseradish peroxidase yields a fully active, homogeneous enzyme, Anal. Biochem. 228 (1995) 48–55.
[34] L. Østergaard, K. Teilum, O. Mirza, O. Mattsson, M. Petersen, K.G. Welinder, J. Mundy, et al., *Arabidopsis* ATP A2 peroxidase: expression and high-resolution structure of a plant peroxidase with implications for lignifications, Plant Mol. Biol. 44 (2000) 231–243.
[35] A. Henriksen, O. Mirza, C. Indiani, K. Teilum, G. Smulevich, K.G. Welinder, M. Gajhede, Structure of soybean seed coat peroxidase: a plant peroxidase with unusual stability and haem-apoprotein interactions, Protein Sci. 10 (2001) 108–115.
[36] O. Mirza, K.G. Welinder, *Arabidopsis thaliana* peroxidase N: structure of a novel neutral peroxidase, Acta Crystallogr. D 56 (2000) 372–375.
[37] A. Henriksen, K.G. Welinder, M. Gajhede, Structure of barley grain peroxidase refined at 1.9-Å resolution, J. Biol. Chem. 273 (1998) 2241–2248.
[38] M. Petrek, P. Kosinova, J. Koca, M. Otyepka, MOLE: a voronoi diagram-based explorer of molecular channels, pores, and tunnels, Structure 15 (2007) 1357–1363.
[39] A.T. Smith, N.C. Veitch, Substrate binding and catalysis in heme peroxidases, Curr. Opin. Chem. Biol. 2 (1998) 269–278.
[40] T.L. Poulos, Thirty years of heme peroxidase structural biology, Arch. Biochem. Biophys. 500 (2010) 3–12.
[41] V. Guallar, B. Olsen, The role of the heme propionates in heme biochemistry, J. Inorg. Biochem. 100 (2006) 755–760.